CrossMark

Hydrothermally Synthesized Co_3O_4, α-Fe_2O_3, and $CoFe_2O_4$ Nanostructures: Efficient Nano-adsorbents for the Removal of Orange G Textile Dye from Aqueous Media

Mostafa Y. Nassar[1] · Talaat Y. Mohamed[1] · Ibrahim S. Ahmed[1] ·
Naglaa M. Mohamed[1] · Mai Khatab[1]

Abstract We herein report the preparation of Co_3O_4, α-Fe_2O_3, and $CoFe_2O_4$ nanostructures through a hydrothermal method followed by a subsequent heat treatment. The as-prepared nanostructures exhibited good adsorption properties for the removal of Orange G (OG) textile dye. Various parameters influencing the adsorption process have been investigated such as contact time, initial dye concentration, ionic strength, adsorbent dose, and temperature. The maximum adsorption capacity values were found to be 33.3, 53.2, and 62.0 mg/g, for Co_3O_4, $CoFe_2O_4$, and α-Fe_2O_3 nano-adsorbents, respectively. The adsorption data fit the pseudo-second-order kinetic and Langmuir isotherm models well. Based on the calculated thermodynamic constants: $\Delta H°$ (3.660, 14.82, and 0.4710 kJ/mol), $\Delta G°$ (from −0.8090 to −1.109, from −0.6444 to −1.682, and from −3.665 to −3.943 kJ/mol), and E_a (9.277, 5.060, and 12.10 kJ/mol), the adsorption of OG dye on the aforementioned nano-adsorbents, respectively, was found to be endothermic, spontaneous, and physisorption process. In addition, because of the relatively high adsorption capacity and chemical stability, the as-synthesized α-Fe_2O_3 adsorbent is suggested as a promising candidate for the removal of OG textile dye from aqueous solutions.

✉ Mostafa Y. Nassar
m_y_nassar@yahoo.com; m_y_nassar@fsc.bu.edu.eg

✉ Talaat Y. Mohamed
prof_talaat2017@yahoo.com

1   Chemistry Department, Faculty of Science, Benha University, Benha 13518, Egypt

1 Introduction

Synthetic organic dyes play a significant role in various industries such as paper, leather, plastic, rubber, and textile dyeing. However, the effluents of these industries include large quantities of toxic and carcinogenic dyes [1, 2]. The release of these dyes into the aquatic environment without pre-treatment causes tremendous problematic issues such as inhibition of the sunlight penetration into the aquatic media, undesirable colors, and several severe diseases. Additionally, these dyes can also cause serious problems on the human health such as respiratory issues, chemical burns, irritation, ulcers, etc. [3–6]. Among these discharged dyes is Orange G dye which is classified as one of the reactive dyes, and this dye is biodegradable and chemically stable. Notably, toxicity and carcinogenicity of these dyes are mainly due to the azo groups (–N=N–) which are included in their molecular structures.

Therefore, because of the serious environmental problems the organic dyes can cause, it is necessary to remove them from wastewater before being discharged into environment. To date, different physical, chemical, and biological methods have been proposed for the removal of the organic dyes from wastewaters. In this light, several methods have been reported such as membrane separation, coagulation, ultra-sonication, photocatalysis, advanced oxidation, biological treatment, coagulation, and adsorption [5, 7–19]. However, due to simple design, high efficiency, scalability, low-cost operation, and wide adaptability of the adsorption process, it still has the superiority among other techniques [20]. In this light, various adsorbent materials such as natural and prepared polymers, zeolites, activated carbons, hydrotalcites, and clays have been proposed for the treatment of wastewater from textile dyes [21–23].

Recently, various research groups have devoted their effort to exploring more suitable adsorbents such as nano-materials which are characterized by high surface area, low-cost production, and high chemical stability [11]. Some metal oxide nanostructures such as ZnO, Fe_2O_3, and Mn_2O_3 have been synthesized by simple procedures and proposed for removal of some reactive dyes such as Reactive Black 5 and Reactive Red 195 dyes from wastewaters because of their nontoxicity and good adsorption capacity [6, 24, 25]. In addition, various nano-materials have been prepared and applied to remove various dyes [26, 27]. However, reports on the removal of Orange G dye from wastewaters are still limited. Moreover, search development of nano-adsorbents with high adsorption capacity and high chemical stability is still a challenge. Notably, metal carbonates have been proved their efficiency in synthesis of various metal oxides which can be used as efficient nano-adsorbents for the removal of some textile dyes from wastewaters [6, 11, 25, 28–30].

Herein, we report on the removal of Orange G dye, as a textile dye pollutant model, using different nano-adsorbents such as hydrothermally synthesized α-Fe_2O_3, Co_3O_4, and $CoFe_2O_4$ nanoparticles. Various factors influencing the adsorption process have been investigated such as contact time, initial pH, initial dye concentration, etc. The kinetics and thermodynamics of the adsorption process were studied as well. The experimental data were examined by employing different isotherm models. Recycling of the hydrothermally synthesized nano-adsorbents was investigated to determine the optimum nano-adsorbent for the removal of OG textile dye in this study.

2 Experimental

2.1 Materials and Reagents

All chemicals and reagents used in the present work were of analytical grade and used without further purification. Ammonium carbonate $[(NH_4)_2CO_3]$ was purchased from Fluka company. Cobalt acetate $[Co(CH_3COO)_2 \cdot 4H_2O]$, iron sulfate $(FeSO_4 \cdot 7H_2O)$, ascorbic acid $(C_6H_8O_6)$, cobalt sulfate $(CoSO_4 \cdot 7H_2O)$, and Orange G dye $(C_{16}H_{10}N_2Na_2O_7S_2,$ $pK_a = 12.8$, and Scheme 1), were supplied by Sigma-Aldrich company.

2.2 Preparation of Adsorbent Nanostructures

2.2.1 Preparation of Co_3O_4 Nanoparticles

Co_3O_4 nanoparticles have been prepared and reported by Mostafa Y. Nassar elsewhere [29]. Briefly, cobalt carbonate nanostructure precursor was synthesized by the
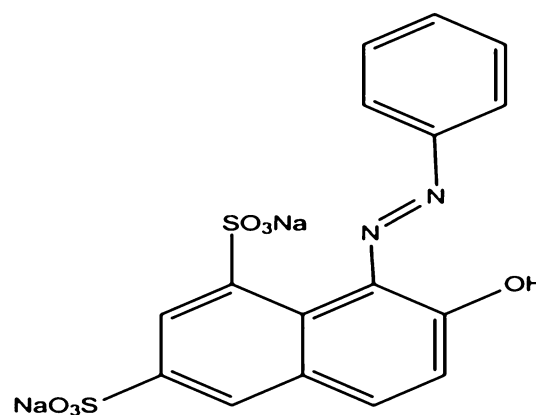
Scheme 1 Chemical structure of Orange G dye

hydrothermal reaction of aqueous solution of ammonium carbonate (2 g, 20.81 mmol, 3 eq.) (60 mL) and an aqueous solution of cobalt acetate $[Co(CH_3COO)_2 \cdot 4H_2O$ (1.728 g, 6.938 mmol, 1 eq.)] (20 mL) in a 100 mL-autoclave at 120 °C for 30 min. Then, the autoclave was left to reach room temperature (~25 °C) naturally. The pink precipitate was collected, washed, and dried at 60 °C for 6 h. Afterward, the hydrothermally prepared $CoCO_3$ nanoparticles were thermally decomposed at 400 °C for 2 h to produce Co_3O_4 nano-adsorbent.

2.2.2 Preparation of α-Fe_2O_3 Nanoparticles

Synthesis and characterization of α-Fe_2O_3 nanostructure were reported by Nassar et al. elsewhere [25]. In brief, $FeCO_3$ nanoparticles were prepared by the hydrothermal treatment of aqueous solutions of iron sulfate (1.95 g, 7 mmol, 1 eq., 20 mL), ascorbic acid (1.23 g, 7 mmol, 1 eq., 20 mL) and ammonium carbonate (2.016 g, 21 mmol, 3 eq., 20 mL) with a molar ratio of 1:1:3, respectively, in 100 mL-autoclave for 1.5 h at 140 °C. Next, the produced iron carbonate precipitate was collected, washed with distilled water then with ethanol, and dried at 60 °C for 6 h. Finally, pure α-Fe_2O_3 nanostructures with a crystallite size of 11 nm were produced through thermal decomposition of the as-prepared iron carbonate at 400 °C for 2 h.

2.2.3 Preparation of Cobalt Ferrite Nanoparticles

Cobalt ferrite $(CoFe_2O_4)$ nanoparticles were previously synthesized as reported by Nassar et al. elsewhere [11]. An aqueous solution (40 mL) of iron sulfate (2.0 g, 7.18 mmol, 0.6 eq.), ascorbic acid (2.11 g, 11.97 mmol, 1 eq.), and cobalt sulfate (1.35 g, 4.79 mmol, 0.4 eq.) was stirred for 5 min. To this stirring solution, ammonium carbonate aqueous solution (20 mL) (3.45 g, 35.91 mmol, 3 eq.) was added and the reaction was stirred for 10 min then transferred to

an autoclave maintained at 140 °C for 3 h. The $FeCO_3$/$CoCO_3$ composite precipitate was isolated, washed with water and ethanol, and dried at 60 °C overnight. Then, cobalt ferrite ($CoFe_2O_4$) nanoparticles were produced by thermal decomposition of the as-prepared carbonate composite precursor at 600 °C for 2 h.

2.3 Characterization

The phase compositions of the as-produced products were characterized by using powder XRD patterns collected by X-ray diffractometer (Bruker; model D8 Advance) attached to a monochromated Cu-Kα radiation (λ = 1.54178 Å). The FE-SEM images of the as-prepared products were collected by using a field emission scanning electron microscope (FE-SEM) equipped with a microscope (JEOL JSM-6390). The TEM images of the as-synthesized products were taken by using a high-resolution transmission electron microscope (HR-TEM) (JEM-2100) with 200 kV accelerating voltage. The FT-IR spectra of the products were recorded from 4000 to 400 cm^{-1} on FT-IR spectrometer (Thermo Scientific; model Nicolet iS10). The UV–Visible spectra of the Orange G dye (OG) were collected by using an UV–Visible spectrophotometer (Jasco; model v670). Thermal study of the as-synthesized carbonate precursors was performed at 15 °C/min heating rate under N_2 gas atmosphere by using a thermal analyzer instrument (Shimadzu; model TA-60WS). The chemical stability of the as-prepared nano-adsorbents was examined by determination of the concentration of the released cobalt and/or iron ions in solutions at the obtained optimum pH value for 24 and 48 h, employing an inductively coupled plasma-optical emission spectrometer (ICP-OES; Optima 7000 DV, PerkinElmer, USA).

2.4 Adsorption Studies

To examine the adsorption efficiency of Co_3O_4, α-Fe_2O_3, and $CoFe_2O_4$ nanoparticles, Orange G dye was selected as a contamination model for textile industry pollutants. The adsorption experiments were carried out employing the batch technique in 250-mL conical flasks under magnetic stirring (400 rpm). Different experimental factors influencing the adsorption process were investigated such as contact time (0–150 min), initial dye concentration (20–250 mg L^{-1}), KCl concentration (0.027–0.295 mol/L), initial pH (1–10) of the dye solution, and temperature (298–328 K). In a typical adsorption experiment, 0.05 g of the as-synthesized adsorbent was added to 50 mL of the dye solution of specific pH which was previously adjusted using 0.2 M NaOH and/or HCl aqueous solutions. The suspension was then magnetically stirred at a specific temperature, for pre-defined time periods. After that, at specific time periods, aliquots were regularly drawn

out from the flask, and the nanoparticles were separated by centrifugation. The absorbance of the supernatant was measured at $λ_{max}$ = 477 nm by using an UV–Vis spectrophotometer to determine the residual dye concentration after adsorption. Finally, the residual dye concentration was estimated by utilizing a previously constructed calibration curve. Notably, the adsorption capacity of the adsorbents [q_t, (mg/g)] and the dye removal percentage (% removal) were determined, using Eqs. (1) and (2).

$$q_t = \frac{V(C_0 - C_t)}{m} \tag{1}$$

$$\%\ removal = \frac{(C_0 - C_t)}{C_0} \times 100 \tag{2}$$

where, C_0 (mg/L) is the initial dye concentration at time = 0, C_t (mg/L) is the remaining dye concentration at time t, V (L) is the volume of the dye solution, and m (g) is the mass of the adsorbent.

3 Results and Discussion

3.1 Synthesis and Characterization of α-Fe_2O_3, Co_3O_4, and $CoFe_2O_4$ Nano-adsorbents

α-Fe_2O_3, Co_3O_4, and $CoFe_2O_4$ nano-adsorbents have proven their efficiency in the removal of methylene blue and Reactive red 195 dyes, as reported elsewhere [8, 11, 25]. Orange G dye as mentioned before is a carcinogenic dye; therefore, we aimed to remove this dye from contaminated aqueous solutions. Hence, we prepared the aforementioned nano-adsorbents to decontaminate wastewaters contaminated with Orange G dye. Figure 1a–c exhibits the XRD patterns of the as-prepared nano-adsorbents: Co_3O_4, α-Fe_2O_3, and $CoFe_2O_4$, respectively. All the diffraction peaks could perfectly be assigned to a pure cubic Co_3O_4 phase (JCPDS card no. 74-1657, space group Fd3m), hexagonal α-Fe_2O_3 phase (JCPDS card no. 89-0598, space group R-3c), and cubic spinel $CoFe_2O_4$ phase (JCPDS card 22-1086, space group Fd-3m), respectively. No diffraction peaks corresponding to any impurities have been observed. The obtained results are consistent with the published data [8, 11, 25, 31]. The other characterization techniques and various properties of the α-Fe_2O_3, Co_3O_4, and $CoFe_2O_4$ nano-adsorbents were described elsewhere [8, 11, 25].

3.2 Adsorption Properties of α-Fe_2O_3, Co_3O_4, and $CoFe_2O_4$ Nanoparticles

In order to remove Orange G dye from contaminated water, we have investigated different factors influencing the efficiency of the dye adsorption process such as the contact
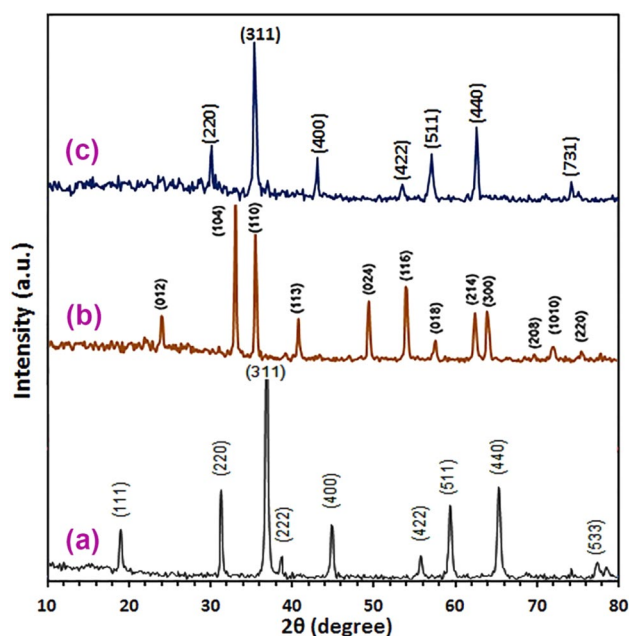
Fig. 1 XRD patterns of the as-prepared Co_3O_4 (*a*), α-Fe_2O_3 (*b*), and $CoFe_2O_4$ (*c*)

Fig. 2 Effect of pH on the adsorption of OG dye on α-Fe_2O_3, Co_3O_4, and $CoFe_2O_4$ nano-adsorbents

time, initial dye concentration, salt effect, initial pH of the dye solution, adsorbent dose, and temperature of the adsorption media.

3.2.1 Effect of pH

Notably, initial pH of the adsorption media has an essential role in the adsorption process owing to its remarkable effect on the electrostatic interaction which can exist between the adsorbent nanoparticles and the adsorbate molecules. Hence, we have examined the influence of initial pH (1–10) of the dye solution on the adsorption process under the experimental conditions: 50 mL of OG dye with an initial concentration (C_0) of 50 mg/L, 0.05 g of nano-adsorbent, for 24 h, and at 25 °C. The data are displayed in Fig. 2. The results exhibited that at lower pH values (i.e. 1–3) the removal dye efficiency enhanced, and the maximum adsorption capacity was attained at pH 3, 2, and 2 for α-Fe_2O_3, Co_3O_4, and $CoFe_2O_4$ nano-adsorbent, respectively. Besides, it was reported that the point of zero charge values for α-Fe_2O_3, Co_3O_4, and $CoFe_2O_4$ nano-adsorbent were 6.8, 7.5, and 7.2, respectively [11, 25, 32]. An important implication of these findings is that these results can be interpreted on the basis of the point of zero charge values of the nano-adsorbents under investigation. Consequently, at low pH values (i.e. $pH < pH_{pzc}$), the electrostatic attraction between the negatively charged OG dye molecules and the positively charged adsorbent nanoparticles was high. Moreover, at pH > 3, the number of positively charged
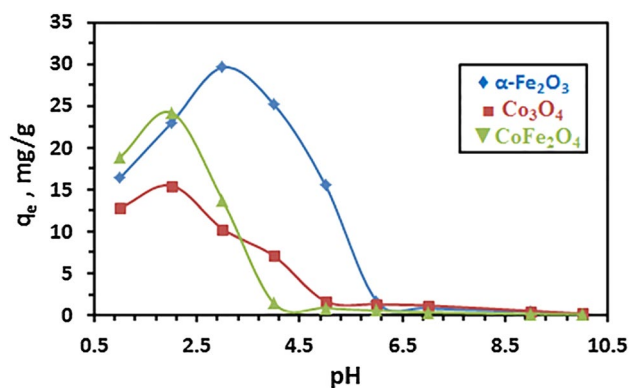
sites diminished, resulting in a decrease in the electrostatic attraction between the oppositely charged species. Afterward, at higher pH values (i.e. $pH > H_{pzc}$), there were repulsive forces between the negatively charged adsorbent nanoparticles and the negatively charged OG dye molecules resulting in low adsorption efficiency values. These results are compatible with other data reported for the adsorption of RR195 and congo red dyes on some nano-adsorbents [11, 25, 33].

3.2.2 Adsorption Kinetics

To determine the optimum time required for the maximum adsorption of OG dye on the as-prepared nano-adsorbents under investigation, we have studied the effect of the contact time (0–150 min) on the dye removal performance under the experimental conditions: 50 mL of OG dye solution with an initial concentration (C_0) of 50 mg/L, nano-adsorbent dose of 0.05 g, at the obtained optimum pH values for the nano-adsorbents (i.e. pH 3, 2, and 2 for α-Fe_2O_3, Co_3O_4, and $CoFe_2O_4$, respectively), and at 25 °C. The results are presented in Fig. 3a. The results showed that the adsorption of the dye started relatively fast. As the contact time elapsed, the removal performance increased until it reached a maximum value at 30 min, and the adsorption capacity then remained constant, indicating a short equilibration time (30 min).

Furthermore, to design and optimize the adsorption process, it is essential to develop the appropriate kinetic model for it. Therefore, to attain profound information about the mechanism and kinetic order of the adsorption of the OG dye on the as-prepared nano-adsorbents, we have adopted three kinetic models to investigate the experimental adsorption results. The applied kinetic models are pseudo-first-order [34], pseudo-second-order [35], and intra-particle diffusion model [36]. The linearized forms of the kinetic
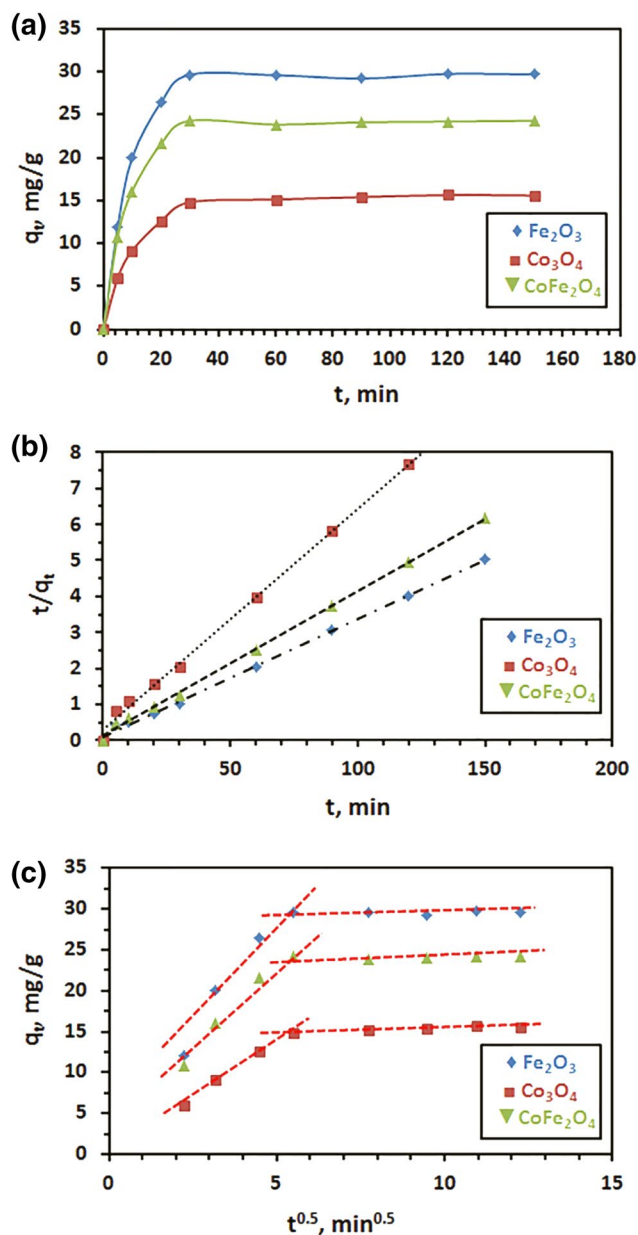
Fig. 3 Influence of contact time (**a**), pseudo-second-order model (**b**), and intra-particle diffusion model (**c**) for the OG dye adsorption on α-Fe$_2$O$_3$, Co$_3$O$_4$, and CoFe$_2$O$_4$ nano-adsorbents

Table 1 Kinetic constants for the adsorption of OG dye on α-Fe$_2$O$_3$, Co$_3$O$_4$, and CoFe$_2$O$_4$ nano-adsorbents

Kinetics models	Constants	α-Fe$_2$O$_3$	Co$_3$O$_4$	CoFe$_2$O$_4$
Pseudo-first-order	K$_1$ (1/min)	0.0458	0.0074	0.0551
	q$_{e(cal)}$ (mg/g)	7.915	12.14	3.910
	r$_1^2$	0.638	0.615	0.407
	q$_{e(exp)}$ (mg/g)	29.6	15.5	24.1
Pseudo-second-order	K$_2$ [g/(mg min)]	0.0075	0.0096	0.0098
	q$_{e(cal)}$ (mg/g)	30.77	16.43	25.10
	r$_2^2$	0.9985	0.9989	0.9989
	q$_{e,exp}$ (mg/g)	29.6	15.5	24.1
	h (mg/mg min)	7.139	2.593	6.146

where, t (min), q$_e$ (mg/g), q$_t$ (mg/g), k$_1$(1/min), k$_2$ (g/mg/min), C (mg/g), and k$_i$ [mg/(g min$^{1/2}$)] are the contact time, equilibrium adsorption capacity of the as-prepared adsorbent, adsorption capacity of the as-prepared adsorbent at time t, pseudo-first-order adsorption rate constant, pseudo-second-order adsorption rate constant, the intercept of the plot of Eq. (5) pointing out the thickness of the boundary layer, and the intra-particle diffusion adsorption rate constant, respectively. The determined kinetic constants, obtained from the previously mentioned models for the adsorption processes under investigation, are presented in Table 1. The rate constant of the pseudo-first-order model was determined from the slope of plotting of log (q$_e$ − q$_t$) against t (not shown) as it is clear from Eq. (3). Moreover, the pseudo-second-order rate constant is calculated from the slope and the intercept of the graph obtained from plotting of t/q$_t$ versus t (Fig. 3b). According to the correlation coefficient (r^2) values presented in Table 1, it is indicated that the experimental results of the adsorption OG dye on the as-prepared nano-adsorbents obey well the pseudo-second-order model. This is because the correlation coefficient (r^2) values for this model are closer to unity (0.997) while those from the pseudo-first-order rate model are in the range of 0.407–0.638. Besides, the calculated adsorption capacity [q$_{e(cal)}$] values obtained by applying the pseudo-second-order model are consistent with the experimentally obtained ones [q$_{e(exp)}$]. Hence, the rate constant of the pseudo-second-order rate model was subsequently used to estimate the initial sorption rate (h) at C$_0$ = 50 mg/L by using Eq. (6) (Table 1) [37].

$$h = k_2 q_e^2 \qquad (6)$$

The results revealed that the initial sorption rate (h) values were in the following order: α-Fe$_2$O$_3$ > CoFe$_2$O$_4$ > Co$_3$O$_4$.

Additionally, to know whether the adsorption process is controlled by a pure diffusion mechanism or not, the Weber and Morris model (Eq. 5) has been adopted.

models can be expressed as presented in Eqs. (3, 4, 5), respectively.

$$\log\left(q_e - q_t\right) = \log q_e - \frac{k_1}{2.303}t \qquad (3)$$

$$\frac{t}{q_t} = \frac{1}{k_2 \, q_e^2} + \frac{t}{q_e} \qquad (4)$$

$$q_t = k_i t^{0.5} + C \qquad (5)$$

Therefore, a plot of q_t against $t^{0.5}$ values was examined. This plot gave a multi-linear curve which did not pass through the origin, as depicted in Fig. 3c. All nano-adsorbents gave similar adsorption results. Hence, it is concluded that the rate determining steps of the adsorption processes are controlled by different mechanisms such as bulk diffusion and film diffusion along with the intra-particle diffusion mechanism [38].

3.2.3 Effect of Ionic Strength

The presence of inorganic salts as stimulators during the dyeing process in the textile industries and releasing them into their industrial wastewaters is a common issue. Therefore, studying the effect of presence potassium chloride in the adsorption media on the adsorption efficiency is an essential factor. The effect of the presence of potassium chloride salt (in the concentration range of 0.027–0.295 mol/L) on the adsorption process efficiency has been studied under the experimental conditions: 50 mL of OG dye with an initial concentration (C_0) of 50 mg/L, 0.05 g of the nano-adsorbent, pH 2 for Co_3O_4 and $CoFe_2O_4$ nano-adsorbents or pH 3 for α-Fe_2O_3 nano-adsorbent, at 25 °C, and for 30 min. The results are presented in Fig. 4. The data depicted in Fig. 4 revealed that the three nano-adsorbents gave similar results. The results exhibited that the dye removal performance decreased with increasing the potassium chloride concentration. This trend can be ascribed to the competition between the small anions (Cl^-) and the negatively charged OG dye molecules for the adsorbent active sites during the adsorption process. This behavior is in good agreement with that reported by other research groups [5, 25, 39].
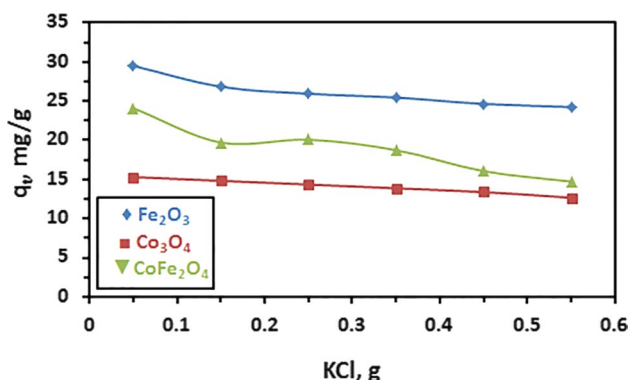
3.2.4 Effect of Adsorbent Dose

The influence of the as-prepared nano-adsorbent dose on the adsorption of OG dye has been investigated, and the results are depicted in Fig. 5. The results revealed that the adsorption efficiency has not been influenced by increasing the amount of $CoFe_2O_4$ nanoparticles. Besides, the adsorption capacity of Co_3O_4 for OG dye enhanced with increasing the Co_3O_4 dose until it reached maximum at 0.075 g; then, it decreased slightly. The enhancement of the adsorption efficiency is probably due to the increase in the adsorption active sites with increasing the adsorbent dose. Then, for an adsorbent dose greater than 0.075 g of Co_3O_4, the adsorbent may undergo agglomeration, resulting in reduction of the surface area of the adsorbent. However, increasing the α-Fe_2O_3 adsorbent dose brought about a decrease in the adsorption performance. The decrease in the adsorption process is probably due to the aggregation that the adsorbent may undergo with increasing its adsorbent dose. This agglomeration may result in a decrease in the surface area of the adsorbent. These results are consistent with the published data [39].

3.2.5 Effect of Initial OG Dye Concentration and Adsorption Isotherm

The effect of varying the initial concentration of OG dye on its adsorption on the as-prepared nano-adsorbents was examined under the experimental conditions: 50 mL of OG dye with various initial concentrations (C_0); 0.05 g of α-Fe_2O_3, and $CoFe_2O_4$ nano-adsorbents or 0.075 g of Co_3O_4 nano-adsorbent; pH 2 for Co_3O_4 and $CoFe_2O_4$ nano-adsorbents or pH 3 for α-Fe_2O_3 nano-adsorbent; at 25 °C; and for 30 min. The obtained data are displayed in Fig. 6a. As seen from Fig. 6, the adsorption capacity of the adsorbent was enhanced when the initial dye concentration increased until it reached maximum [$q_{e(exp)}$ = 30.0, 40.0, and 48.5 mg/g] at initial dye concentrations of 150, 150,

Fig. 4 Effect of potassium chloride concentration on the adsorption of OG dye on α-Fe_2O_3, Co_3O_4, and $CoFe_2O_4$ nano-adsorbents
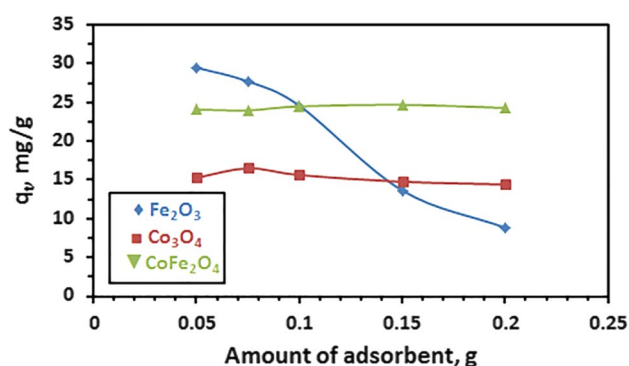
Fig. 5 Effect of adsorbent dose on the adsorption of OG dye on α-Fe_2O_3, Co_3O_4, and $CoFe_2O_4$ nano-adsorbents
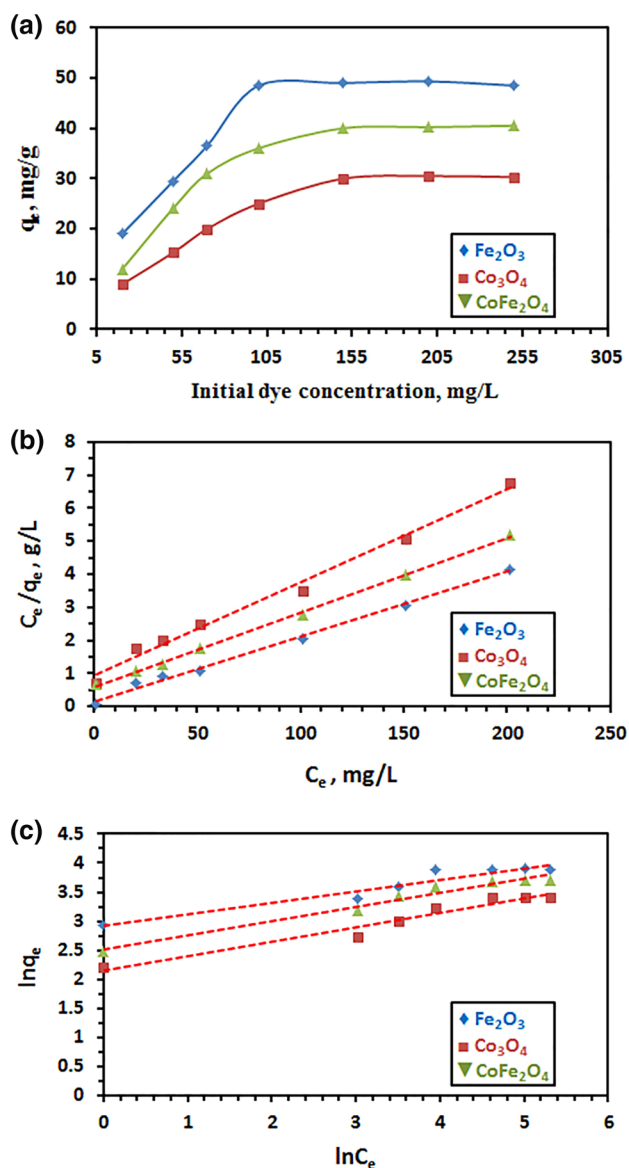
Fig. 6 Effect of initial dye concentration (**a**), Langmuir isotherm model (**b**), and Freundlich isotherm model (**c**) for the adsorption of OG dye on α-Fe_2O_3, Co_3O_4, and $CoFe_2O_4$ nano-adsorbents

and 100 mg/L, for Co_3O_4, $CoFe_2O_4$, and α-Fe_2O_3 nano-adsorbents, respectively. The enhancement in the amount of the adsorbed quantity with increasing the initial dye concentration is probably owing to the increase in the concentration gradient driving force. The constancy of the adsorption capacity at higher dye concentrations might be due to the saturation of the surface sites available for the adsorption process. These results are in good agreement with the reported results [11, 39].

Furthermore, the adsorption results have been examined by employing two well-known adsorption isotherms; Langmuir and Freundlich isotherm models, to explore the OG dye adsorption mechanism. Where, the Langmuir model

is applied to adsorption on homogenous surfaces, and the Freundlich model is used for adsorption on heterogeneous surfaces. The linearized forms of the Langmuir and Freundlich isotherm models can be expressed by Eqs. (7) and (8), respectively.

$$\frac{C_e}{q_e} = \frac{1}{K_L q_m} + \frac{C_e}{q_m} \tag{7}$$

$$\ln q_e = \ln K_F + \frac{1}{n} \ln C_e \tag{8}$$

where, C_e (mg/L) is the equilibrium concentration of the OG dye, q_e (mg/g) is the OG dye adsorbed quantity at equilibrium, K_L (L/mg) is the Langmuir constant, q_m (mg/g) is the nano-adsorbent maximum adsorption capacity for OG dye, K_F [(mg/g)(L/mg)$^{1/n}$] is the Freundlich constant, and n is a constant (suggesting the adsorption intensity which can be deduced from the Freundlich isotherm model). According to the Langmuir isotherm model (Eq. 7), the constants, q_m and K_L, can be calculated from the intercept and the slope of the plot of C_e/q_e versus C_e, as displayed in Fig. 6b. Additionally, based on the Freundlich isotherm model (Eq. 8), K_F and n constants can be estimated from the slope and the intercept of the plot of $\ln q_e$ versus $\ln C_e$, as depicted in Fig. 6c. Although it is known that the q_m value can be calculated by using the Langmuir isotherm equation (as mentioned before), q_m can be also estimated utilizing the Freundlich isotherm model by using Eq. (9), based on the published data by Halsey [40].

$$K_F = \frac{q_m}{C_0^{1/n}} \tag{9}$$

The determined parameters of both isotherm models are presented in Table 2. It is clear from Table 2 that the experimental adsorption results follow well the Langmuir isotherm model, and this is mainly based on the correlation coefficient values (r^2) of the isotherm models of interest. Furthermore, the determined maximum adsorption capacities obtained from the Langmuir isotherm model are consistent with the experimentally calculated ones. The results also indicate the adsorbent homogenous nature and monolayer coverage of the adsorption of OG dye on the as-prepared adsorbents.

In addition, the adsorption performance of OG dye on the as-prepared adsorbents was examined by employing the dimensionless constant, R_L, (Eq. 10).

$$R_L = \frac{1}{1 + K_L C_0} \tag{10}$$

where, C_0 (mg/L) is the initial OG dye concentration, and K_L (L/mg) is the Langmuir constant. The R_L constant

Table 2 Langmuir and Freundlich isotherm parameters for the adsorption of OG dye on α-Fe₂O₃, Co₃O₄, and CoFe₂O₄ adsorbents

Adsorption isotherm	Parameters	α-Fe$_2$O$_3$	Co$_3$O$_4$	CoFe$_2$O$_4$
Langmuir	K_L (L/mg)	0.135	0.0398	0.0530
	$q_{m(cal)}$ (mg/g)	50.9	34.8	44.9
	r_1^2	0.995	0.992	0.998
	R_L	0.0289–0.271	0.0914–0.557	0.0702–0.485
	$q_{e(exp)}$ (mg/g)	48.5	30.0	40.0
Freundlich	K_F [(mg/g)(L/mg)$^{1/n}$]	18.8	4.67	6.81
	$q_{m(cal)}$ (mg/g)	46.0	31.0	42.6
	r_2^2	0.921	0.957	0.887
	n	5.14	2.65	2.73
	$q_{e,(exp)}$ (mg/g)	48.5	30.0	40.0

values give an indication whether the adsorption process is favorable ($0 < R_L < 1$), linear ($R_L = 1$), irreversible ($R_L = 0$), or unfavorable ($R_L > 1$) [41]. In the current investigation, the determined R_L values were in the range of 0.271–0.0288, 0.557–0.0914, and 0.485–0.0701 for the initial concentration range of 20–250 mg/L, indicating that the adsorption of OG dye on α-Fe₂O₃, Co₃O₄, and CoFe₂O₄ adsorbents, respectively, is a favorable process.

3.2.6 Adsorption Thermodynamics

The influence of temperature on the adsorption of OG dye on the as-prepared nano-adsorbents was studied in a temperature range of 298–318 K under the optimum adsorption conditions: 50 mL of OG dye with various initial concentrations (C_0), 0.05 g of α-Fe₂O₃ and CoFe₂O₄ nano-adsorbents or 0.075 g of Co₃O₄ nano-adsorbent, pH 2 for Co₃O₄ and CoFe₂O₄ nano-adsorbents or pH 3 for α-Fe₂O₃ nano-adsorbent, for 30 min, and at 298, 308, or 318 K temperature. Interestingly, all the adsorbents showed an increase in the adsorption capacity with increasing the temperature of the adsorption media indicating the endothermic nature of the adsorption under investigation, as displayed in Fig. 7a. In addition, to get further insight into the adsorption process, we have calculated some thermodynamic constants to get information about the energy changes related to the adsorption process. Consequently, some thermodynamic constants have been determined such as enthalpy change ($\Delta H°$), Gibbs free energy change ($\Delta G°$), and entropy change ($\Delta S°$), utilizing Eqs. (11) and (12) [25].

$$\ln K_c = \frac{\Delta S°}{R} - \frac{\Delta H°}{RT} \qquad (11)$$

$$\Delta G° = \Delta H° - T\Delta S° \qquad (12)$$

where, T and R are the absolute temperature of the adsorption medium (K) and the universal gas constant (8.314×10^{-3} kJ/mol K), respectively. Besides, K_c is the thermodynamic equilibrium constant; however, this
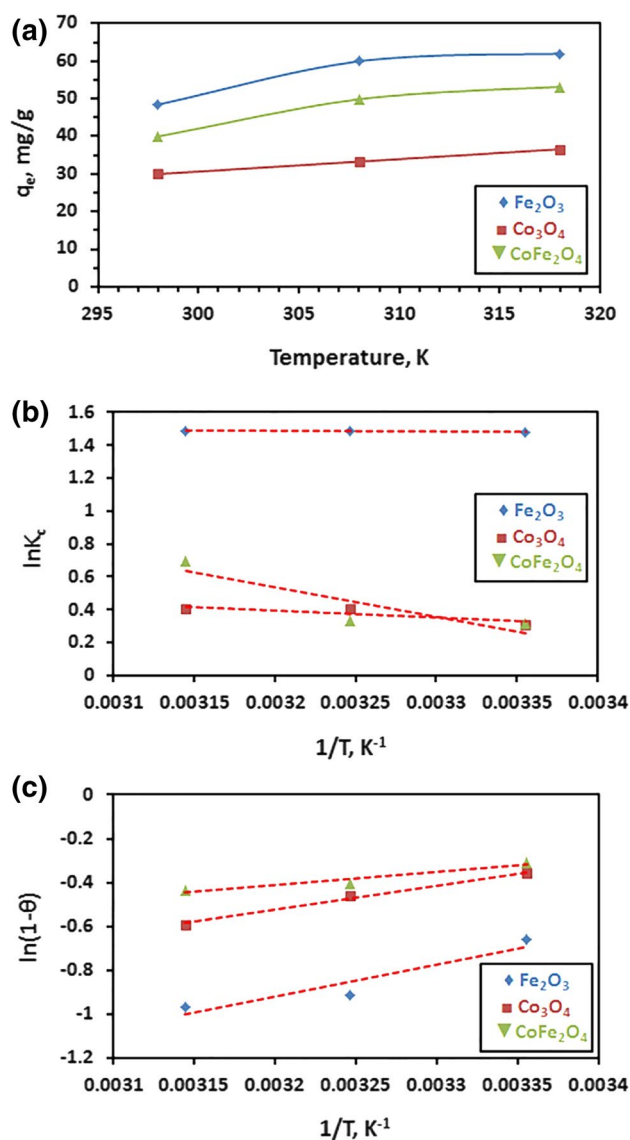
Fig. 7 Effect of temperature (**a**), plot $\ln K_c$ versus 1/T (**b**), and plot of $\ln(1 - \theta)$ versus 1/T (**c**) for the adsorption of OG dye on α-Fe₂O₃, Co₃O₄, and CoFe₂O₄ nano-adsorbents

constant value should be dimensionless. This comes from the fact that $\Delta G°$, T, and R units appeared in Eq. (13) are in kJ/mol, K, and kJ/mol K, respectively. Therefore, some routes have been suggested for the calculation of a dimensionless thermodynamic equilibrium constant [42–47].

$$\Delta G° = RTlnK_c \qquad (13)$$

In the present study, we have determined the dimensionless thermodynamic equilibrium constant (K_c) by employing the partition constant (K_p) [5, 43, 48].

As proposed by Niwas et al. [43], the thermodynamic equilibrium constant (K_c) can be expressed by Eq. (14).

$$K_c = \frac{a_s}{a_e} = \frac{\gamma_s}{\gamma_e}\frac{C_s}{C_e} \qquad (14)$$

where, a_e and a_s are the activity of the dye in solution at equilibrium and the activity of the adsorbed dye, respectively. Besides, C_e and C_s are the equilibrium concentration of the adsorbate in solutions and the adsorbed quantity of the adsorbate on the adsorbent, respectively. In addition, γ_e and γ_s are the activity coefficient of the dye in solution at equilibrium and the activity coefficient of the adsorbed dye, respectively. In a highly dilute concentration of a solute, the solute concentration goes to zero in that solution, and the activity coefficient goes to unity. Therefore, Eq. (14) can be approximated to Eq. (15). Hence, the partition coefficient (K_p) and the thermodynamic equilibrium constant (K_c) are of equal values, and the partition coefficient is in unison with the unit of that thermodynamic constant.

$$K_p = \frac{C_s}{C_e} = \frac{a_s}{a_e} = K_c \qquad (15)$$

The K_p constant (i.e. $K_c = K_p$ in the current case) can be determined by plotting $ln(C_s/C_e)$ against C_s, and extrapolating C_s to zero to give an intercept which is equal to K_c [48]. Afterward, the constants $\Delta H°$ and $\Delta S°$ can be determined from the slope and the intercept of the plot of lnK_c against 1/T (Fig. 7b). Moreover, $\Delta G°$ value can be estimated by

substituting $\Delta H°$ and $\Delta S°$ with their values in Eq. (12). The estimated thermodynamic constants are tabulated in Table 3.

The listed thermodynamic constants in Table 3 exhibit that the adsorption processes of the OG dye on the as-prepared nano-adsorbents are spontaneous and endothermic based on the obtained positive and negative values for $\Delta H°$ and $\Delta G°$, respectively. Additionally, the results also showed that the adsorption process at higher temperatures was thermodynamically favorable because $\Delta G°$ values increased in the negative direction with rising the temperature. In addition, according to the calculated values of $\Delta H°$ (from 0.4710 to 14.82 kJ/mol) and $\Delta G°$ (from −0.6444 to −3.943 kJ/mol), it was concluded that the adsorption of OG dye on the nano-adsorbents under investigation was physisorption as $\Delta H°$ and $\Delta G°$ values lay in the range of <40 kJ/mol and (−20)−(0) kJ/mol, respectively.

Moreover, in order to confirm the physisorption nature of the adsorption process, we have calculated the activation energy (E_a) by using the modified Arrhenius equation [Eq. (16)] related to surface coverage (θ) for OG dye adsorption on the as-prepared nano-adsorbents [9, 49].

$$S^* = (1 - \theta)e^{-\frac{E_a}{RT}} \qquad (16)$$

where, S^* ($0 < S^* < 1$) is an adsorbate/adsorbent function (sticking probability), and this function depends on temperature. C_0 and C_e parameters have the aforementioned definitions. θ can be replaced with $[1 - C_e/C_0]$ in Eq. (16). Taking natural logarithms of both sides of Eq. (16) produces Eq. (17)

$$ln(1 - \theta) = lnS^* + E_a/RT \qquad (17)$$

From the slope and the intercept of the plot of $ln(1 - \theta)$ versus 1/T (Fig. 7c), we have determined the activation energy (E_a) of the adsorption process. Notably, E_a values were estimated to be 5.060, 9.277, and 12.10 kJ/mol for the adsorption of OG dye on α-Fe_2O_3, Co_3O_4, and $CoFe_2O_4$

Table 3 Thermodynamic parameters for the adsorption of OG dye on α-Fe_2O_3, Co_3O_4, and $CoFe_2O_4$ nano-adsorbents

Adsorbent	Method	T (K)	K_c	$\Delta G°$ (kJ/mol)	$\Delta S°$ (J/mol K)	$\Delta H°$ (kJ/mol)	r^2	E_a (kJ/mol)	S^*
α-Fe_2O_3	Partition constant, K_p ($K_p = K_c$)	298	4.385	−3.665	0.0139	0.4710	0.907	12.10	3.78×10^{-3}
		308	4.427	−3.804					
		318	4.438	−3.943					
Co_3O_4	Partition constant, K_p ($K_p = K_c$)	298	1.367	−0.8090	0.0150	3.660	0.800	9.277	16.6×10^{-3}
		308	1.494	−0.9590					
		318	1.499	−1.109					
$CoFe_2O_4$	Partition constant, K_p ($K_p = K_c$)	298	1.375	−0.6444	0.0519	14.82	0.770	5.060	94.2×10^{-3}
		308	1.396	−1.163					
		318	2.011	−1.682					

adsorbents, respectively. Therefore, this indicates that the adsorption of OG dye on the as-prepared adsorbents is a physisorption process because the values are in the range of 5–40 kJ/mol reported for the physisorption [6, 50]. This conclusion is consistent with that obtained from the $\Delta G°$ and $\Delta H°$ values, supporting the physisorption nature of the adsorption processes under study.

3.2.7 The Reusability of the As-Prepared Adsorbents and Comparison with Others

From an economic point of view, the regeneration of the α-Fe_2O_3, Co_3O_4, and $CoFe_2O_4$ adsorbents and their reusability for OG dye adsorption are important factors for the application purposes. Hence, we have investigated the regeneration and reusability of the as-prepared adsorbents. Adsorption of OG dye on the as-prepared nano-adsorbents was achieved under the obtained optimum adsorption conditions; subsequently, the OG dye-loaded nano-adsorbent was regenerated by its stirring in an aqueous dye solution at pH 10 for 3 h, followed by centrifugation then washing with water and methanol. The regenerated adsorbent was then dried for 6 h at ca. 70 °C. The adsorption–desorption procedure was repeated five times, and the obtained results were depicted in Fig. 8. The results showed that the as-prepared adsorbents (α-Fe_2O_3, Co_3O_4, and $CoFe_2O_4$) still have good reproducibility and adsorption performance (ca. 91, 90, and 92%, respectively), after even five cycles of regeneration. Consequently, the collected results indicate that the as-prepared nano-adsorbents can be proposed as good candidates for the removal of OG dye from aqueous media and also support the long-term use of the nano-adsorbents. On the other hand, Table 4 lists the maximum adsorption capacities (q_m) of different adsorbents for the removal of OG dye. The tabulated results reveal that the as-prepared α-Fe_2O_3 adsorbent has a relatively high q_m value in comparison to the q_m values of the other listed adsorbents in Table 4. In addition, the as-prepared Co_3O_4, α-Fe_2O_3, and

Table 4 Comparison between the maximum adsorption capacities of several adsorbents toward the removal of OG dye

Adsorbent material	Adsorption capacities, q_m, mg/g	Reference
Hematite	630.0×10^{-3}	[51]
Modified sawdust	5.480	[52]
MgO nanoparticles	21.50	[1]
Magnetic Biochar	32.36	[53]
Co_3O_4 nanoparticles	33.30	The present study
$CoFe_2O_4$ nanoparticles	53.20	The present study
α-Fe_2O_3 nanoparticles	62.00	The present study
Mesoporous carbon CMK-3	189.0	[54]

$CoFe_2O_4$ adsorbents exhibited high chemical stability because the analyzed concentrations of the released cobalt and/or iron ions from the adsorbents, at the corresponding pH value, were estimated to be ca. 0.025 for cobalt ions, 0.005 for iron ions, and (0.020 for cobalt ions and 0.001 for iron ions) mg/L, respectively, after 24 h contact time. And the released cobalt and iron ions concentrations (at the corresponding pH value, and after 48 h contact time) were determined to be ca. 0.053 for cobalt ions, 0.011 for iron ions, and (0.048 for cobalt ions and 0.002 for iron ions) mg/L, respectively. Consequently, low concentrations of the leached ions from the as-prepared adsorbents will not bring about an environmental metal pollution.

Although one of the listed adsorbents has a higher q_m value, the as-prepared α-Fe_2O_3 adsorbent has many characteristics such as 100% desorption ratio, five-cycle reusability, high chemical stability, and low-cost production. Actually, all these characteristics stimulated us to propose this adsorbent as a good candidate for the removal of OG dye from aqueous media.

4 Conclusions

In conclusion, α-Fe_2O_3, Co_3O_4, and $CoFe_2O_4$ nanostructures were successfully synthesized using a hydrothermal method followed by a subsequent heat treatment at 400 °C or 600 °C for 2 h. This was achieved using inexpensive ammonium carbonate as a carbonate source at relatively low temperatures (120 and 140 °C) for relatively short time (30 min or 3 h). The as-prepared nanostructures: Co_3O_4, $CoFe_2O_4$, and α-Fe_2O_3, revealed a high adsorption capacity: ca. 33.3, 53.2, and 62.0 mg/g, respectively, toward the removal of orange G (OG) textile dye. Besides, the adsorption results fit well the pseudo-second-order and Langmuir adsorption isotherm models. In addition, the intra-particle diffusion and other mechanisms such as the bulk diffusion and film diffusion mechanisms contributed
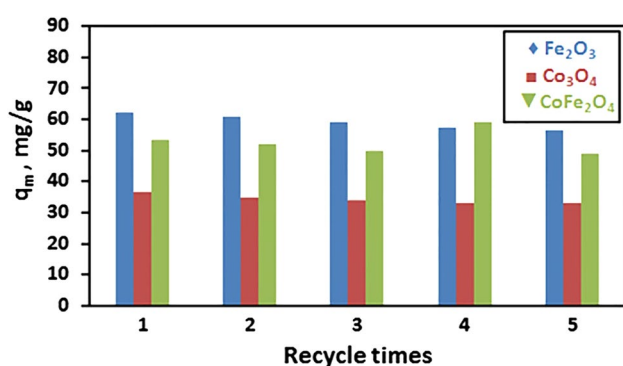

Fig. 8 Regeneration efficiency of α-Fe_2O_3, Co_3O_4, and $CoFe_2O_4$ nano-adsorbents for the removal of OG dye

to the adsorption mechanism. Moreover, the adsorption of OG dye on the as-prepared nano-adsorbents depended on the temperature of the adsorption medium, and the process was spontaneous, physisorption, and endothermic, according to the calculated thermodynamic constants. Eventually, the findings indicate that the as-prepared α-Fe$_2$O$_3$ nanoparticles can be proposed as a promising candidate for the removal of OG dye from aqueous solutions.

References

1. M.Y. Nassar, T.Y. Mohamed, I.S. Ahmed, I. Samir, MgO nanostructure via a sol–gel combustion synthesis method using different fuels: an efficient nano-adsorbent for the removal of some anionic textile dyes. J. Mol. Liq. **225**, 730–740 (2017)

2. T.A. Khan, S. Dahiya, I. Ali, Use of kaolinite as adsorbent: Equilibrium, dynamics and thermodynamic studies on the adsorption of Rhodamine B from aqueous solution. Appl. Clay Sci. **69**, 58–66 (2012)

3. N.F. Cardoso, R.B. Pinto, E.C. Lima, T. Calvete, C.V. Amavisca, B. Royer, M.L. Cunha, T.H.M. Fernandes, I.S. Pinto, Removal of remazol black B textile dye from aqueous solution by adsorption. Desalination **269**, 92–103 (2011)

4. B. Kayan, B. Gözmen, M. Demirel, A.M. Gizir, Degradation of acid red 97 dye in aqueous medium using wet oxidation and electro-Fenton techniques. J. Hazard. Mat. **177**, 95–102 (2010)

5. M.Y. Nassar, E.I. Ali, E.S. Zakaria, Tunable auto-combustion preparation of TiO$_2$ nanostructures as efficient adsorbents for the removal of an anionic textile dye. RSC Adv. **7**, 8034–8050 (2017)

6. M.Y. Nassar, M.M. Moustafa, M.M. Taha, Hydrothermal tuning of the morphology and particle size of hydrozincite nanoparticles using different counterions to produce nanosized ZnO as an efficient adsorbent for textile dye removal. RSC Adv. **6**, 42180–42195 (2016)

7. J. Huang, Y. Cao, Z. Liu, Z. Deng, W. Wang, Application of titanate nanoflowers for dye removal: a comparative study with titanate nanotubes and nanowires. Chem. Eng. J. **191**, 38–44 (2012)

8. M.Y. Nassar, I.S. Ahmed, Template-free hydrothermal derived cobalt oxide nanopowders: synthesis, characterization, and removal of organic dyes. Mater. Res. Bull. **47**, 2638–2645 (2012)

9. H.R. Mahmoud, S.M. Ibrahim, S.A. El-Molla, Textile dye removal from aqueous solutions using cheap MgO nanomaterials: Adsorption kinetics, isotherm studies and thermodynamics. Adv. Powder Technol. **27**, 223–231 (2016)

10. R.G. Saratale, G.D. Saratale, J.S. Chang, S.P. Govindwar, Bacterial decolorization and degradation of azo dyes: a review. J. Taiwan Inst. Chem. Eng. **42**, 138–157 (2011)

11. M.Y. Nassar, M. Khatab, Cobalt ferrite nanoparticles via a template-free hydrothermal route as an efficient nano-adsorbent for potential textile dye removal. RSC Adv. **6**, 79688–79705 (2016)

12. M.Y. Nassar, I.S. Ahmed, I. Samir, A novel synthetic route for magnesium aluminate (MgAl$_2$O$_4$) nanoparticles using sol–gel auto combustion method and their photocatalytic properties. Spectrochim. Acta Part A Mol. Biomol. Spectrosc. **131**, 329–334 (2014)

13. T. Jiao, H. Guo, Q. Zhang, Q. Peng, Y. Tang, X. Yan, B. Li, Reduced graphene oxide-based silver nanoparticle-containing composite hydrogel as highly efficient dye catalysts for wastewater treatment. Sci. Rep. **5**, 11873 (2015)

14. M.Y. Nassar, A.A. Ali, A.S. Amin, A facile Pechini sol-gel synthesis of TiO$_2$/Zn$_2$TiO$_2$/ZnO/C nanocomposite: an efficient catalyst for the photocatalytic degradation of Orange G textile dye. RSC Adv. **7**, 30411–30421 (2017)

15. J. Zhang, M. Chen, L. Zhu, Activation of persulfate by Co$_3$O$_4$ nanoparticles for orange G degradation. RSC Adv. **6**, 758–768 (2016)

16. J. Zhang, M. Chen, L. Zhu, Activation of peroxymonosulfate by iron-based catalysts for orange G degradation: role of hydroxylamine. RSC Adv. **6**, 47562–47569 (2016)

17. M.Y. Nassar, H.M. Aly, M.E. Moustafa, E.A. Abdelrahman, Synthesis, characterization and biological activity of new 3-substitued-4-amino-5-hydrazino-1,2,4-triazole schiff bases and their Cu(II) complexes: a new approach to CuO nanoparticles for photocatalytic degradation of methylene blue dye. J. Inorg. Organomet. Polym. Mater. (2017). doi:10.1007/s10904-017-0569-x

18. M.Y. Nassar, H.M. Aly, E.A. Abdelrahman, M.E. Moustafa, Synthesis, characterization, and biological activity of some novel Schiff bases and their Co(II) and Ni(II) complexes: a new route for Co$_3$O$_4$ and NiO nanoparticles for photocatalytic degradation of methylene blue dye. J. Mol. Struct. **1143**, 462–471 (2017)

19. H.M. Aly, M.E. Moustafa, M.Y. Nassar, E.A. Abdelrahman, Synthesis and characterization of novel Cu(II) complexes with 3-substituted-4-amino-5-mercapto-1,2,4-triazole Schiff bases: a new route to CuO nanoparticles. J. Mol. Struct. **1086**, 223–231 (2015)

20. K.B. Tan, M. Vakili, B.A. Horri, P.E. Poh, A.Z. Abdullah, B. Salamatinia, Adsorption of dyes by nanomaterials: recent developments and adsorption mechanisms. Sep. Purif. Technol. **150**, 229–242 (2015)

21. Y.S. Al-Degs, M.I. El-Barghouthi, A.H. El-Sheikh, G.M. Walker, Effect of solution pH, ionic strength, and temperature on adsorption behavior of reactive dyes on activated carbon. Dyes Pigm. **77**, 16–23 (2008)

22. C.-K. Lee, S.-S. Liu, L.-C. Juang, C.-C. Wang, K.-S. Lin, M.-D. Lyu, Application of MCM-41 for dyes removal from wastewater. J. Hazard. Mat. **147**, 997–1005 (2007)

23. A. Nematollahzadeh, A. Shojaei, M. Karimi, Chemically modified organic/inorganic nanoporous composite particles for the adsorption of reactive black 5 from aqueous solution. React. Funct. Polym. **86**, 7–15 (2015)

24. M.Y. Nassar, A.S. Amin, I.S. Ahmed, S. Abdallah, Sphere-like Mn$_2$O$_3$ nanoparticles: facile hydrothermal synthesis and adsorption properties. J. Taiwan Inst. Chem. Eng. **64**, 79–88 (2016)

25. M.Y. Nassar, I.S. Ahmed, T.Y. Mohamed, M. Khatab, A controlled, template-free, and hydrothermal synthesis route to sphere-like [small alpha]-Fe$_2$O$_3$ nanostructures for textile dye removal. RSC Adv. **6**, 20001–20013 (2016)

26. O.A. Attallah, M.A. Al-Ghobashy, M. Nebsen, M.Y. Salem, Removal of cationic and anionic dyes from aqueous solution with magnetite/pectin and magnetite/silica/pectin hybrid nanocomposites: kinetic, isotherm and mechanism analysis. RSC Adv. **6**, 11461–11480 (2016)

27. A. El-Qanni, N.N. Nassar, G. Vitale, Experimental and computational modeling studies on silica-embedded NiO/MgO nanoparticles for adsorptive removal of organic pollutants from wastewater. RSC Adv. **7**, 14021–14038 (2017)

28. M.Y. Nassar, S. Abdallah, Facile controllable hydrothermal route for a porous CoMn$_2$O$_4$ nanostructure: synthesis, characterization, and textile dye removal from aqueous media. RSC Adv. **6**, 84050–84067 (2016)

29. M.Y. Nassar, Size-controlled synthesis of CoCO$_3$ and Co$_3$O$_4$ nanoparticles by free-surfactant hydrothermal method. Mater. Lett. **94**, 112–115 (2013)

30. M.Y. Nassar, I.S. Ahmed, Hydrothermal synthesis of cobalt carbonates using different counter ions: an efficient precursor to nano-sized cobalt oxide (Co_3O_4). Polyhedron **30**, 2431–2437 (2011)

31. M.Y. Nassar, T.Y. Mohamed, I.S. Ahmed, One-pot solvothermal synthesis of novel cobalt salicylaldimine-urea complexes: a new approach to Co_3O_4 nanoparticles. J. Mol. Struct. **1050**, 81–87 (2013)

32. M. Kosmulski, Compilation of PZC and IEP of sparingly soluble metal oxides and hydroxides from literature. Adv. Colloid Interface Sci. **152**, 14–25 (2009)

33. S. Yavari, N.M. Mahmodi, P. Teymouri, B. Shahmoradi, A. Maleki, Cobalt ferrite nanoparticles: preparation, characterization and anionic dye removal capability. J. Taiwan Inst. Chem. Eng. **59**, 320–329 (2016)

34. M.N. Sepehr, V. Sivasankar, M. Zarrabi, M. Senthil Kumar, Surface modification of pumice enhancing its fluoride adsorption capacity: an insight into kinetic and thermodynamic studies. Chem. Eng. J. **228**, 192–204 (2013)

35. Y.S. Ho, G. McKay, Pseudo-second order model for sorption processes. Process Biochem. **34**, 451–465 (1999)

36. W.J. Wber, J.C. Morris, *Proceedings of the International Conference on Water Pollution Symposium*. (Pergamon Press, Oxford, 1962)

37. F.A. Batzias, D.K. Sidiras, Dye adsorption by prehydrolysed beech sawdust in batch and fixed-bed systems. Bioresour. Technol. **98**, 1208–1217 (2007)

38. C. Luo, Z. Tian, B. Yang, L. Zhang, S. Yan, Manganese dioxide/iron oxide/acid oxidized multi-walled carbon nanotube magnetic nanocomposite for enhanced hexavalent chromium removal. Chem. Eng. J. **234**, 256–265 (2013)

39. N.M. Mahmoodi, F. Najafi, Preparation of surface modified zinc oxide nanoparticle with high capacity dye removal ability. Mater. Res. Bull. **47**, 1800–1809 (2012)

40. G.D. Halsey, The Role of Surface Heterogeneity in Adsorption, ed. by V.I. Komarewsky, W.G. Frankenburg, E.K. Rideal, *Advances in Catalysis*, (Academic Press, London, 1952), pp. 259–269

41. T.G. Venkatesha, R. Viswanatha, Y. Arthoba Nayaka, B.K. Chethana, Kinetics and thermodynamics of reactive and vat dyes adsorption on MgO nanoparticles. Chem. Eng. J. **198–199**, 1–10 (2012)

42. Y. Liu, Is the free energy change of adsorption correctly calculated? J. Chem. Eng. Data **54**, 1981–1985 (2009)

43. R. Niwas, U. Gupta, A.A. Khan, K.G. Varshney, The adsorption of phosphamidon on the surface of styrene supported zirconium(IV) tungstophosphate: a thermodynamic study. Colloids Surf. A **164**, 115–119 (2000)

44. S.K. Milonjić, A consideration of the correct calculation of thermodynamic parameters of adsorption. J. Serb. Chem. Soc. **72**, 1363–1367 (2007)

45. X. Zhou, X. Zhou, The unit problem in the thermodynamic calculation of adsorption using the Langmuir equation. Chem. Eng. Commun. **201**, 1459–1467 (2014)

46. P.S. Ghosal, A.K. Gupta, Determination of thermodynamic parameters from Langmuir isotherm constant-revisited. J. Mol. Liq. **225**, 137–146 (2017)

47. H.N. Tran, S.-J. You, H.-P. Chao, Thermodynamic parameters of cadmium adsorption onto orange peel calculated from various methods: a comparison study. J. Environ. Chem. Eng. **4**, 2671–2682 (2016)

48. A.A. Khan, R.P. Singh, Adsorption thermodynamics of carbofuran on Sn(IV) arsenosilicate in H^+, Na^+ and Ca^{2+} forms. Colloids Surf. **24**, 33–42 (1987)

49. M. Ghaedi, A. Hekmati Jah, S. Khodadoust, R. Sahraei, A. Daneshfar, A. Mihandoost, M.K. Purkait, Cadmium telluride nanoparticles loaded on activated carbon as adsorbent for removal of sunset yellow. Spectrochim. Acta Part A Mol. Biomol. Spectrosc. **90**, 22–27 (2012)

50. J. Ma, Y. Jia, Y. Jing, Y. Yao, J. Sun, Kinetics and thermodynamics of methylene blue adsorption by cobalt-hectorite composite. Dyes Pigm. **93**, 1441–1446 (2012)

51. M.K. Mondal, S. Singh, M. Umareddy, B. Dasgupta, Removal of Orange G from aqueous solution by hematite: isotherm and mass transfer studies. Korean J. Chem. Eng. **27**, 1811–1815 (2010)

52. S. Banerjee, M.C. Chattopadhyaya, Y. Chandra Sharma, Removal of an azo dye (Orange G) from aqueous solution using modified sawdust. J. Water Sanit. Hyg. Dev. **5**, 235–243 (2015)

53. N.M. Mubarak, Y.T. Fo, H.S. Al-Salim, J.N. Sahu, E.C. Abdullah, S. Nizamuddin, N.S. Jayakumar, P. Ganesan, Removal of methylene blue and Orange-G from waste water using magnetic biochar. Int. J. Nanosci. **14**, 1550009 (2015)

54. K.A.V.E.H. Arzani, B.G. Ashtiani, A.H.A. Kashi, Equilibrium and kinetic adsorption study of the removal of Orange-G Dye using carbon mesoporous material. J. Inorg. Mater. **27**, 660–666 (2012)